Annu. Rev. Fluid Mech. 1998. 30:579–612

MICRO-ELECTRO-MECHANICAL-SYSTEMS (MEMS) AND FLUID FLOWS

Chih-Ming Ho
Mechanical and Aerospace Engineering Department, University of California at Los Angeles, Los Angeles, California 90095; e-mail: chihming@seas.ucla.edu

Yu-Chong Tai
Electrical Engineering Department, California Institute of Technology, Pasadena, California 91125; e-mail: yctai@touch.caltech.edu

KEY WORDS: flow control, MEMS, micro transducers, size effect, surface force

ABSTRACT

The micromachining technology that emerged in the late 1980s can provide micron-sized sensors and actuators. These micro transducers are able to be integrated with signal conditioning and processing circuitry to form micro-electro-mechanical-systems (MEMS) that can perform real-time distributed control. This capability opens up a new territory for flow control research. On the other hand, surface effects dominate the fluid flowing through these miniature mechanical devices because of the large surface-to-volume ratio in micron-scale configurations. We need to reexamine the surface forces in the momentum equation. Owing to their smallness, gas flows experience large Knudsen numbers, and therefore boundary conditions need to be modified. Besides being an enabling technology, MEMS also provide many challenges for fundamental flow-science research.

1. INTRODUCTION

During the past decade, micromachining technology has become available to fabricate micron-sized mechanical parts. Micromachines have had a major impact on many disciplines (e.g. biology, medicine, optics, aerospace, and mechanical and electrical engineering). In this article, we limit our discussion to transport phenomena, specifically emphasizing fluid-dynamics issues. This

0066-4189/98/0115-0579$08.00

emerging field not only provides miniature transducers for sensing and actuation in a domain that we could not examine in the past, but also allows us to venture into a research area in which the surface effects dominate most of the phenomena.

Figure 1 shows a scanning-electronic-microscope (SEM) picture of an electrostatically driven motor (Fan et al 1988a). This device signifies the beginning of the micromachine field. A comb structure (Tang et al 1989) derived from the micro motor concept eventually evolved into the airbag sensor, which reduces the damage caused by automobile collisions and is used now on almost all American-made cars. During the development of the micro motor, it was found that the frictional force between the rotor and the substrate is a function of the contact area. This result departs from the traditional frictional law (i.e. $f = \mu N$), which says that the frictional force is linearly proportional to the normal force, N, only. In the micro motor case, the surface forces between the rotor and the substrate contribute to most of the frictional force. However, the traditional frictional law describes situations with a dominating body force that do not depend on the contact area. Deviations from the conventional wisdom are commonly found in the micro world. This makes the micromachine field a new technology as well as a new scientific frontier.

The micromachining process uses lithography to expose the designed photoresist patterns; the unwanted portion is then selectively etched away. These procedures are similar to those used in integrated circuit (IC) fabrication but with

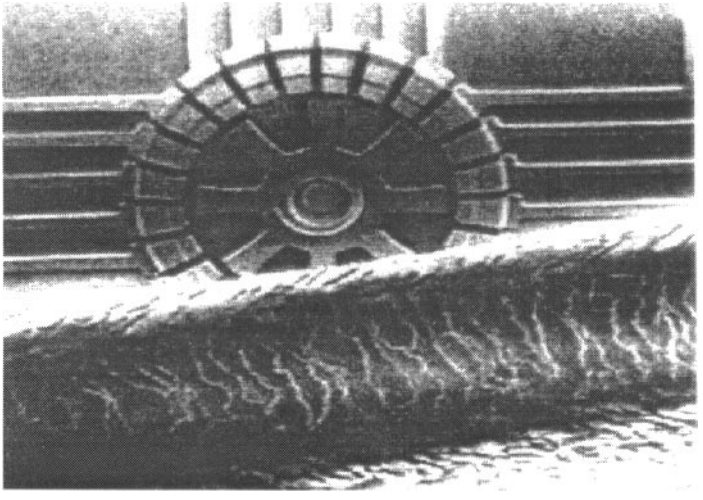

Figure 1 A micro motor (Fan et al 1988a). A piece of human hair is shown in front of the motor to illustrate its minute size.

a difference: 3-D and freestanding structures are common features, because of the nature of mechanical parts. Several manufacturing technologies such as bulk micromachining, surface micromachining, and LIGA (acronym for the German phrase *LIthographe, Galvanoformung, und Abformung*) have been developed to make various micromachines. A brief introduction of these technologies can be found in a paper by Ho & Tai (1996). For detailed information, readers are referred to Petersen 1982, Seidel 1987, and Ristic 1994.

Micromachines have several unique features. First, typical micromachined transducer sizes are on the order of 100 microns, which can be one or more orders of magnitude smaller than traditional sensors and actuators. The drastic reduction in inertia resulting from these smaller sizes means a substantial increase in the frequency response. Second, batch processing—which is characteristic of IC fabrication—can be used to make many transducers for distributed sensing and actuation over a wide area. This capability enables us to sense certain flow characteristics in a 2-D domain and to perform control at the proper locations. Potential application areas include the manipulation of separation over a smooth contour or the reduction of surface shear stress in a turbulent boundary layer. Third, micromachine manufacturing technology is derived from, although not completely compatible with, IC fabrication so it is possible to integrate the IC with micro transducers to provide logic capability. Integrated microelectronics and micromachines constitute the micro-electro-mechanical-system (MEMS), which can execute sense–decision–actuation on a monolithic level.

In biomedical applications, fluid transport is commonly required in drug delivery and in chemical and DNA analyses. When dealing with flow in configurations of microns or less, we have observed many unexpected phenomena that are similar to the aforementioned experience of frictional force between solid surfaces. Sir Eddington (1928) once said "We used to think that if we know one, we know two, because one and one are two. We are finding that we must learn a great deal more about '*and*'." Indeed, the flows in macro *and* micro configurations are not quite the same. The unique features in micromechanics are perhaps the most intriguing ones for researchers in basic fluid mechanics. We still have a great deal of difficulty in understanding these features, because not much is known about the complex surface effects that play major roles in these events. The search for their answers will excite researchers for years to come. In this paper, we first report and discuss the fundamental micro-fluid-mechanics issues and then review flow sensing and control using MEMS.

2. SIZE EFFECTS

2.1 *Ratio Between Surface Force and Body Force*

Length scale is a fundamental quantity that dictates the type of forces governing physical phenomena. Body forces are scaled to the third power of the length

scale. Surface forces depend on the first power or the second power of the characteristic length. Because of the difference in slopes, the body force must intersect with the surface force. In biological studies (Went 1968), empirical observations indicated that a millimeter length is the approximate order of the demarcation. Experiences gathered in MEMS also show that surface forces dominate in sizes smaller than a millimeter. For example, the friction experienced by the 100-micron-diameter micro motor (Fan et al 1988a,b) must be caused mainly by the surface force, because the rotor started to move when the contact area between the rotor and the substrate was reduced by placing dimples on the lower surface of the rotor.

2.2 *Ratio Between Device and Intrinsic Length Scales*

Besides the large surface force, the large surface-to-volume ratio is another characteristic inherent in small devices. This ratio is typically inversely proportional to the smaller length scale of the cross section of the device and is about one micron in surface micromachined devices. Therefore, the surface-to-volume ratio is much larger in a micro device than in a macro device, which accentuates the role of surface force as well as other surface effects in general.

In micro flows, the Reynolds number is typically very small and shows the ratio between the viscous force and the inertial force. However, in the case when gas is the working fluid, the size can be small enough to further modify the viscous effect when the device length scale is on the order of the mean free path. For large Knudsen-number flows, the flow velocity at the surface starts to slip (Knudsen 1909, Kennard 1938); therefore, the viscous shear stress is much reduced. For liquid flows, the distance between molecules is on the order of angstroms. The non-slip condition has always been used as an empirical result. By using a molecular dynamics approach (Koplik et al 1989, Koplik & Banavar 1995), the non-slip condition at the solid surface is established in Couette and Poiseuille liquid flows. On the other hand, molecular ordering has been observed and results in oscillatory density profiles in the vicinity of the wall, which are a few molecular spacings thick. In the case of a moving contact line at the fluid/fluid/solid interface, the non-slip condition needs to be relaxed (Dussan & Davis 1974). Typical micromachined devices have a length scale much larger than the molecular spacing of simple liquids. Hence, the non-slip boundary condition should hold in the absence of a moving contact line.

In other situations, the bulk flow instead of the boundary condition is modified. For example, most solid surfaces have electrostatic surface charges, which can attract ions in liquid flows to form an electric double layer (EDL) (see Section 3.2). The thickness of the EDL varies from a few nm to 100s of nm (Hunter 1981), which can be comparable to the order of micro-flow length

scale. In these cases, the bulk flow can be affected by this electrically charged layer (Mohiuddin Mala et al 1996).

3. SURFACE FORCES

For fluid flows in MEMS, new phenomena arise because of certain surface forces that are usually ignored in macro scales. Here, a brief survey is given on several kinds of surface forces (Israelachvili 1991). Before the discussion of some seemingly different surface forces, it is important to know that these forces originate from intermolecular forces. Moreover, even though basic intermolecular forces are short range (<1 nm) in nature, they can cumulatively lead to very long-range (>0.1 μm) effects (e.g. surface-tension effects in liquids). Another important point is that all intermolecular forces are fundamentally electrostatic (coulombic). This is established by the Hellman-Feynman theorem that states that once the spatial electron distribution is determined from the Schrödinger equation, all intermolecular forces can then be calculated using classical electrostatics. However, in practice this cannot always be done, and empirical or semiempirical laws of forces are still useful. In the following, we then treat the following surface forces differently even though they are the same in origin from the point of view of quantum mechanics.

3.1 *Van der Waals Forces*

The van der Waals forces are the weakest among all the forces, but they are important because they are always present. The van der Waals forces are short range in nature but, in cases where large molecules or surfaces are involved, they can produce an effect longer than 0.1 μm. In general, van der Waals forces have three parts: orientation force, induction force, and dispersion force. All have an interaction free energy that varies with the inverse sixth power of the distance ($1/r^6$) and are, hence, short range. The orientation force is the dipole–dipole interaction force between polar molecules. The induction force arises from the interaction between a polar molecule and a nonpolar molecule. The permanent dipole of the polar molecule induces a weak dipole in the nonpolar molecule and then produces a dipole-induced dipole-interaction force. The dispersion force is then the induced-dipole–induced-dipole interaction force. Interestingly, the dispersion forces act on all atoms and molecules even when they are totally neutral, as are those of helium and oxygen. The source of the dispersion force between two nonpolar molecules is the following: Although the averaged dipole moment of a nonpolar molecule is zero, at any instant there exists a finite dipole moment depending on the exact position of the electrons around its nucleus. This instantaneous dipole moment can then generate an interaction force with nearby molecules.

Altogether, van der Waals forces play an important role in many macroscopic phenomena (e.g. adhesion, surface tension, physical adsorption, wetting of surfaces, properties of thin films, and behaviors of condensed proteins and polymers). In MEMS, the van der Waals forces can have significant effects in structures with large surface-to-volume ratios (e.g. long and thin polysilicon beams [Mastrangelo & Hsu 1992]) and large-and-thin comb-drive structures [Tang et al 1989]) whenever they are in contact with another surface. Stiction or adhesion of the structure to the substrate can often be observed as a major problem in the operation of these structures. Nevertheless, the van der Waals forces between two contacting surfaces are in many cases hard to be separately distinguished from electrostatic (coulombic) forces, which are discussed in the next section.

3.2 *Electrostatic Forces*

Electrostatic, or coulombic, force is present between charged molecules or particles. The force has an inverse-square dependence on the distance, $1/r^2$, so it is rather long range when compared to the van der Waals forces. In MEMS devices, the electrostatic force can have a significant effect even up to 10 μm away and becomes more important when lengths are less than 0.1μm. One can always produce an electrostatic force by providing an electrical potential difference between two electrodes. However, problems deriving from electrostatic force in MEMS often occur because of rather uncontrollable surface-trapped charges. In fact, any surface is likely to carry some charge, because of broken bonds and surface charge traps. In the case where the surface is a good insulator, such as with SiO_2, trapped charges can induce very high voltage from a few hundreds to a few thousands of volts (Wolf 1990).

For charged surfaces in liquids (e.g. water), new phenomena happen mainly as a result of charge redistribution in the liquid. Basically, the final surface charge is balanced by counterions in the liquid by an equal but opposite total charge. The surface electrical potential attracts counterions to the wall and forms a thin (<1 nm) layer of immobile ions. Outside this layer, the distribution of the counterions in liquid mainly followed the exponential decaying dependence away from the surface. This is called the diffuse electric double layer (EDL). EDL has a characteristic length (Debye length), which depends inversely on the square root of the ion concentration in the liquid. For example, in pure water the Debye length is about 1 μm; in 1 mole of NaCl solution, the Debye length is only 0.3 nm. Inside the EDL, a very large electrostatic force then exists. This may cause a behavior change in the fluid flow if the double layer thickness is significant compared to the flow field size (Mohiuddin Mala et al 1996). This is especially true in dilute solutions where the Debye length is large.

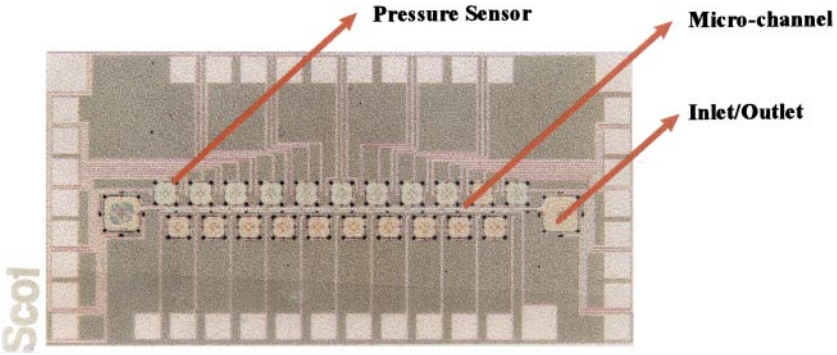

Figure 2 A micro channel system with integrated micro pressure sensors (Pong et al 1994)

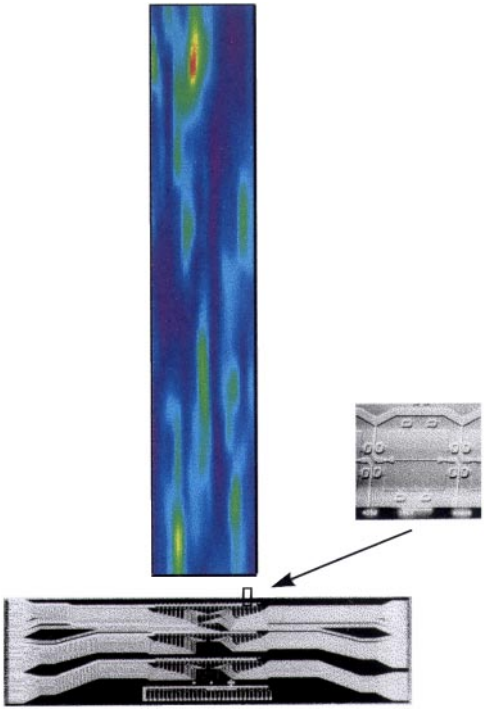

Figure 18 Instantaneous surface shear stress measured by an imaging chip (Ho et al 1997).

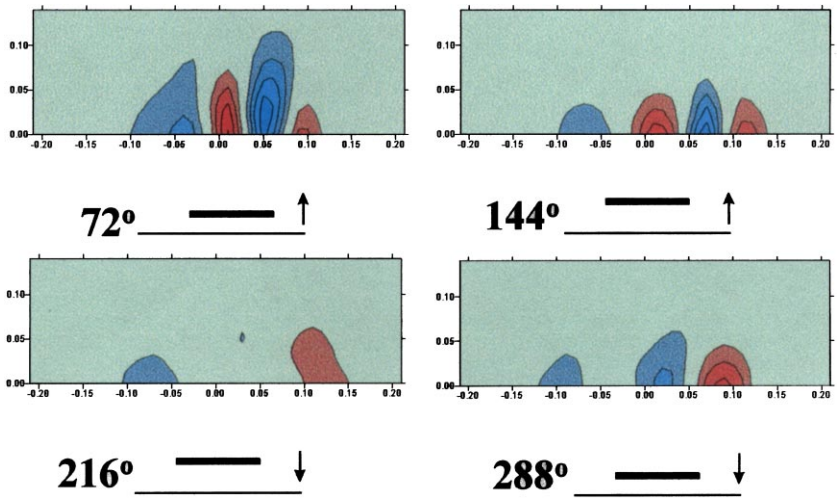

Figure 19 Vertical velocity contours of an flap actuator interacting with a longitudinal vortex pair. The phase angle: *0°* and *360°* flap on the surface; *180°* flap at its upmost location.

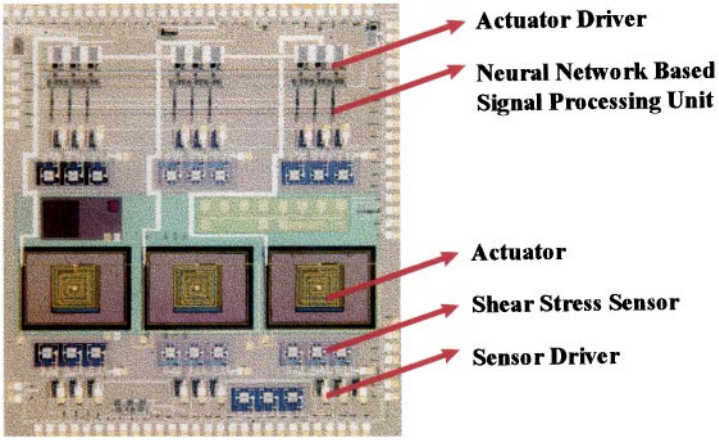

Figure 22 A micro system for surface shear-stess reduction (Ho et al 1997).

3.3 *Steric Forces*

This is a special case involving chain molecules (e.g. polymers) attached at the surface on one end with the other end dangling into the solution (liquid for most of the cases), where they are mobile. A different class of forces, known as steric forces, arises whenever another molecule or surface approaches and is a result of an entropy change caused by the confined chain molecules. The complex molecules can produce complex interactions, and steric forces can be either attractive or repulsive. They can be rather long range ($>0.1\mu$m), and they are important when a fluid flow has a significant amount of long-chain molecules.

4. FLOWS IN MICRO CONFIGURATIONS

Fluids driven by pumps flowing through channels and valves are generic configurations in biomedical analytical systems. When the sizes of these devices are in the micron range, the measured data show different behaviors from those expected in larger devices. The exact physical mechanisms are not known, although the surface forces, which were not considered in classical analyses, are believed to be responsible for these interesting phenomena. This provides a new domain for research opportunities. In this review, we limit the discussion to simple fluids, which have small molecules. More complex fluids (e.g. non-Newtonian or multiphase fluids) are commonly used in biomedical systems. Much richer findings are expected in the future.

4.1 *Gas Flows in Micro Channels*

Flow through a straight channel is one of the simplest but most common configurations in micro fluidic systems. Mass flow rates in small channels with diameters of about 30 microns were measured by Knudsen (1909) while studying the non-slip/slip boundary condition. Recent interests are triggered by micromachine activities (Pfahler et al 1990), which include applications for transporting fluids in biomedical diagnosis and electronic device cooling (Tuckermann & Pease 1982, Joo et al 1995). Helium is a common gas used in most experiments because it has a large mean free path (about 2×10^{-7} m under laboratory conditions). The Knudsen number based on a channel height of 1 micron is 0.2. A micro channel with integrated micro pressure sensors (Figure 2, color insert) was fabricated to study the flow field (Liu et al 1993b, Pong et al 1994). Slip flow is observed, and the measured mass flow rate (Pfahler et al 1991, Pong et al 1994, Arkilic et al 1995, Harley et al 1995, Liu et al 1995, Shih et al 1995, 1996) is higher than that based on the non-slip boundary condition (Figure 3).

For other gases (e.g. nitrogen, oxygen, and nitrous oxide), the Knudsen number is about a factor of four smaller, but surface slip still exits. The mass

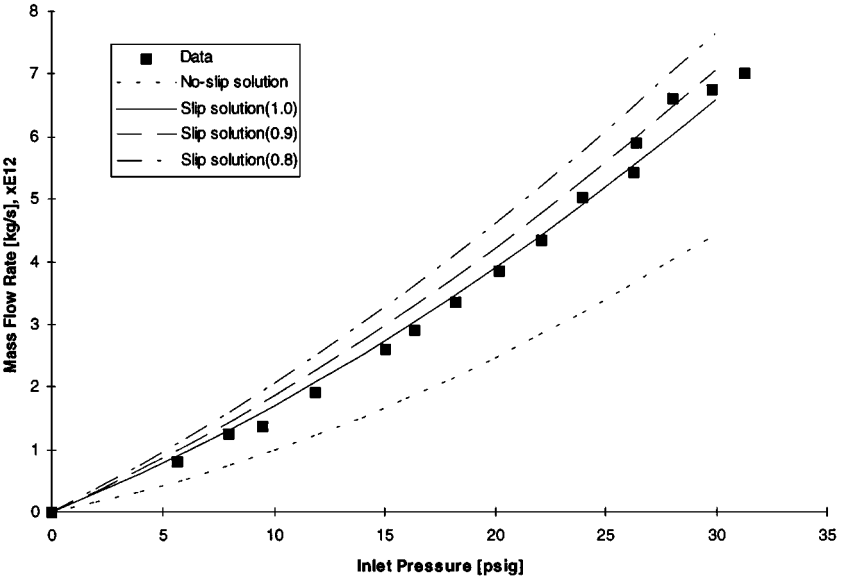

Figure 3 Mass flow rate and pressure drop of helium in a micro channel (Shih et al 1996).

flow rate can be calculated from the Navier-Stokes equation with a slip boundary condition (Kennard 1938, Beskok & Karniadakis 1992 & 1993, Arkilic & Breuer 1993). An accommodation constant is introduced to represent the tangential momentum transfer between the impinging molecules and the wall. The value of the constant should be ≤ 1. However, the predicted mass flow rate is sensitive to the accommodation constant (Figure 3), which actually functions as a matching coefficient. Direct simulation of the Monte Carlo method (DSMC) has been carried out by many investigators (Oh et al 1995, Piekos & Breuer 1995, 1996, Beskok et al 1996, Oran et al 1998). The mean streamwise velocity in the micro channel is typically in the very low subsonic range (<1 m/s), which can be several orders of magnitude smaller than the molecular thermal velocity of 1000 m/s (Oh et al 1995). Computing the converging solution is a challenge for very low Mach-number flows.

In the micro channel, high pressure drops are observed. This is because of the small transverse dimension, which causes high viscous dissipation. A drop of a few atmospheres in pressure of several mm is common (Pong et al 1994, Shih et al 1995). The density of the gas can change so much that the pressure does not decrease linearly with streamwise distance as in typical creeping flows. Rather,

the compressibility effect causes the pressure to decrease more slowly. On the other hand, the rarefaction effect caused by the high Knudsen number works against the compressibility and keeps the pressure toward the linear distribution (Arkilic & Breuer 1993). The two effects are not equal, so the net result is a nonlinear pressure distribution.

Because the pressure distribution is not sensitive to the accommodation constant, it turns out to be a useful property for examining the analytical results. When the accommodation constant is varied, no appreciable change in the predicted pressure distribution can be observed. The measured pressure distributions along the channel are plotted against the theoretical prediction. The measured pressure distribution agrees well with the analytical result (Figure 4).

4.2 *Liquid Flows in Micro Channels*

Even though the non-slip boundary of simple liquids with molecules is established by experimental studies and by molecular dynamics simulation (Koplik 1989), this does not make the study of liquid flow through micro channels a routine process. On the contrary, it seems to be an even richer problem than gas flow. For liquid flows through capillary tubes (Migun & Prokhorenko 1987) or micromachined channels (Pfahler et al 1990, 1991), the measured flow rates and pressure drops across the channel were compared with the Stokes flow solution.

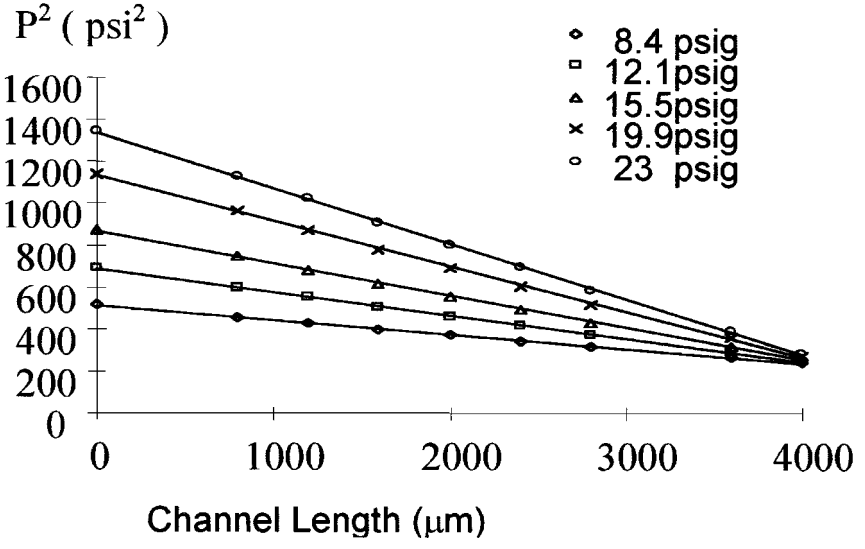

Figure 4 Pressure distribution of nitrous oxide in a micro channel.

Viscosity is the matching constant. Size effects are apparent in these results. The value of viscosity deviates from the conventional value for micron-size channels.

The molecular structure of the liquid also affects the flow. Molecules with no electrical charge can have a dipole configuration (e.g. water). Pfahler et al (1991) found that the value of the viscosity of polar isopropanol decreases from the nominal value for a channel height smaller than 40 microns and reaches an asymptotic value at a channel height of about 10 microns (Figure 5). The vertical axis is the ratio between the apparent viscosity and nominal viscosity. It is reasonable that the size effect becomes more pronounced for a narrow channel.

However, it is interesting to note that the apparent viscosity is lower, not higher, in the narrower channel. The apparent viscosity actually represents the integral effects of the surface forces. More definitive experiments are needed to identify the role of specific surface effects. For example, when the surface-to-volume ratio gets large, will the surface viscous force also be a function of the surface property (i.e. hydrophobic or hydrophilic)? For nonpolar silicon oil, the data (Figure 5) cannot support a clear trend of viscosity variation in this range of channel size.

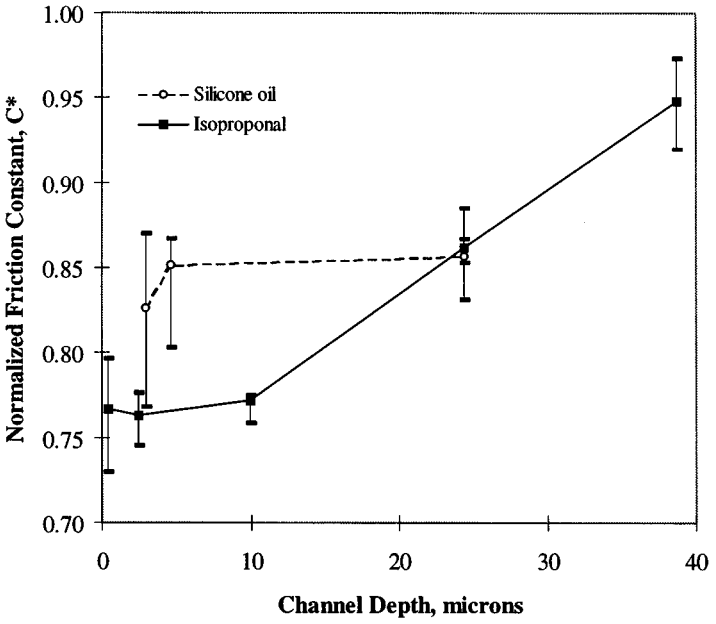

Figure 5 Size effect on liquid flow in channels (Pfahler et al 1991).

4.3 *Diffusion in Micro Channels*

The sacrificial etching technique (Nathanson 1967, Preston 1972, Howe & Muller 1983) is a fundamental technique used in surface micromachining for producing a free-standing structure, such as the diaphragm above a cavity or cantilever beam. The micro channel shown in Figure 2 was fabricated by this method. The sacrificial etching process for making that channel was to deposit a thin line of sacrificial material—in this case phosphosilicate glass (PSG)—after which a structural layer of silicone nitride was placed on top. Hydrofluoric acid (HF) was used as an etchant to remove the PSG from one end of this thin line. When the PSG was etched away, a long micro channel was formed (Monk et al 1993, Liu et al 1993a). The channel in Figure 2 is 1.2 microns high and 4000-microns long.

This process is an important micromachine manufacturing technique, and it also motivates us to examine mass diffusion in micro geometries. The HF diffuses from the reservoir, which is located at one end of the micro channel, towards the PSG/HF interface. The rate at which the solid PSG dissolves into the HF acid is a function of the reaction rate and the concentration of the acid. The concentration of HF at the moving interface is dictated by the diffusion process and the reaction rate. Basically, this phenomenon is governed by a 1-D diffusion equation with an unknown boundary condition. It is similar to the Deal-Grove problem, but the reaction rate changes its power dependence on the acid concentration (Judge 1971) in the present case.

Nevertheless, a closed-form analytical solution can be obtained (Liu 1993a), and it matches well with the measured data (Figure 6). On the other hand, a size effect is observed. The etch rate is not a constant during the etching and decreases as etching time increases. During the whole etching period, the etch rate of a thicker channel is always higher than that of a thin channel (Liu et al 1993a). The etch rate at the beginning of the etching process is plotted in Figure 7 and decreases almost linearly with the channel thickness in the tested range of 1.2 to 0.25 microns. This is not expected from the 1-D diffusion analysis. There are many types of ions in the liquid phase. It is possible that the presence of the EDL affects the etch rate. The F^- ions and HF_2^- ions are responsible for removing the PSG, and their diffusion is very likely to be retarded by the electric double layer.

4.4 *Flow Through Micro Nozzles*

Flow through a nozzle experiences viscous dissipation. In the case of Stokes flow, the pressure drop increases with decreasing Reynolds number—a well-established result. A recent experiment (Hasegawa et al 1997) shows that the predicted pressure drop underestimates the measured value when the size of the nozzle is smaller than 35 microns (Figure 8). The excess pressure

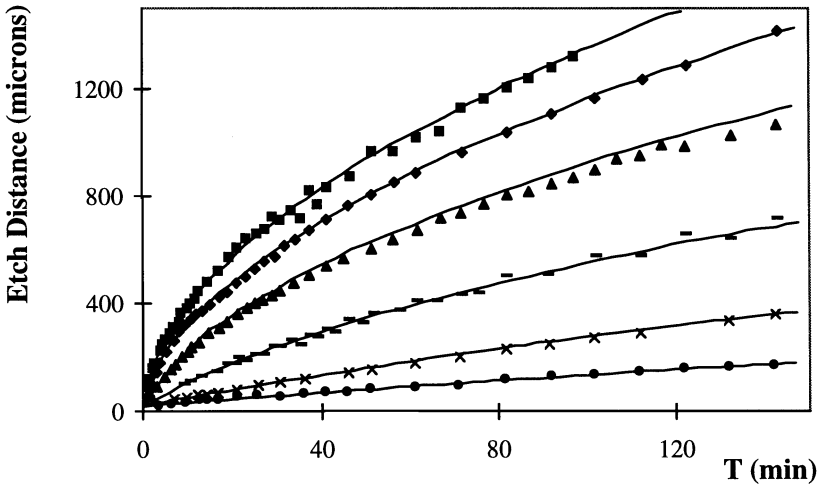

Figure 6 The progress of the etching front as a function of time for various HF concentrations (Liu et al 1993a). ■ = 49%; ◆ = 38.2%; ▲ = 26.5%; — = 13.8%; × = 7.2%; ● = 3.6%. Data points are plotted against predicted curves.

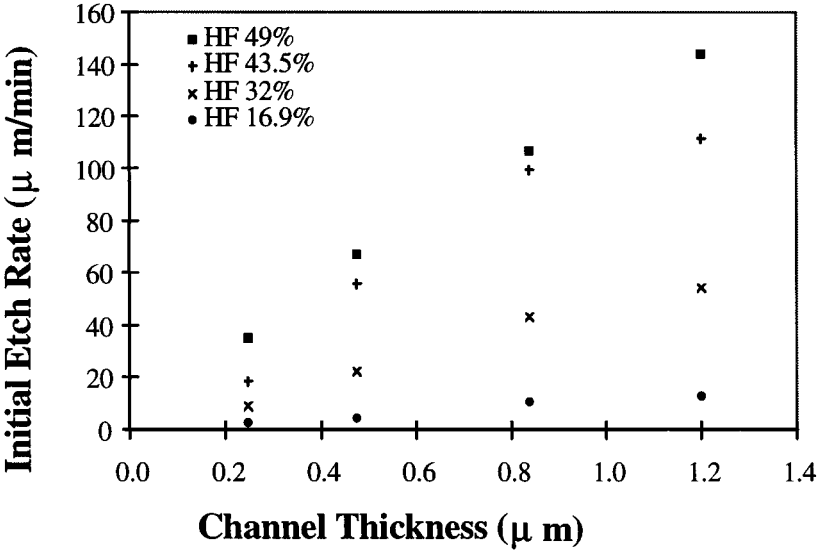

Figure 7 Size effect as a function of etching rate.

drop can be a factor of four or five times higher than the predicted value for water flow through an 8.8-micron nozzle. When nonpolar silicon oil was used, the excess pressure drops were lower than that of water, which has polar molecules. The dependence of the measured flow property on the fluids used in the test is a common feature in micro flows whenever a size effect is observed. It is interesting to note that differences between polar and nonpolar materials, which have been reported in micro channel flow (Pfahler et al 1991), are again observed in this flow.

It has been reported that the EDL retards the flow. This causes an apparent viscosity that is higher than the nominal viscosity (Mohiuddin Mala et al 1996). This is the opposite of the results observed in the micro-channel liquid-flow data (Pfahler et al 1991) but follows the trends reported in the micro-nozzle flow experiment (Hasegawa et al 1997). In this nozzle experiment, the ion content in the water was varied by adding NaCl in order to examine the effect of the EDL. No discernible difference in the pressure measurements was reported by the authors. Unfortunately, distilled water rather than deionized water was used

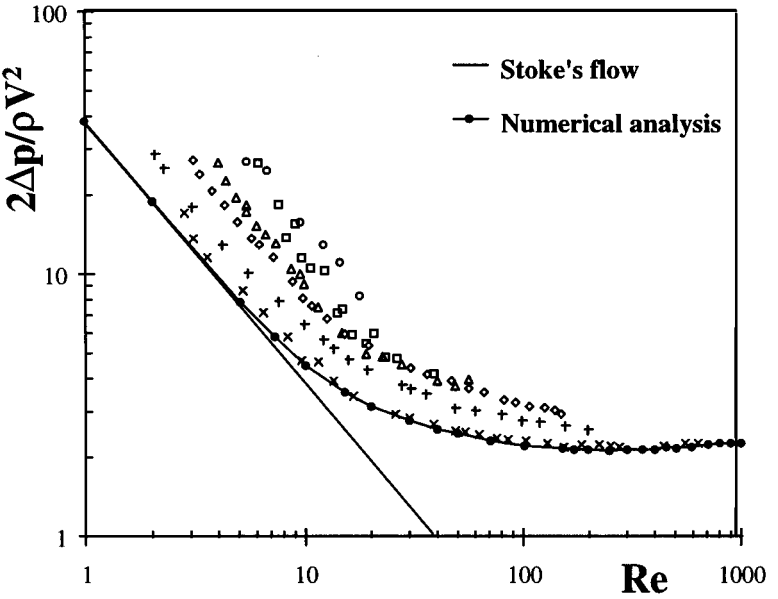

Figure 8 Size effect of pressure drop across micro nozzles as a function of Reynolds number (Hasegawa et al 1997). o, 8.8 μm; Δ, 13 μm; $\diamond$, 27 μm; $+$, 35 μm; $\times$, 109 μm; $\bullet$, numerical simulation.

before the NaCl was added. Water is known to contain ions easily, but the level of the ion content in their distilled water is unknown. Nevertheless, the excess pressure drop across the micro nozzle provides additional evidence for the size effect in the micro flows.

4.5 *Air Damping in MEMS*

Mechanical or electromechanical resonant devices have been widely used in oscillators or filters, and operational theories for these devices have been established in large apparatus. As MEMS technology develops, these resonators are becoming smaller. These devices are typically 1- to 2-μm thick and about 100×100 μm^2 in area. Some important milestones for these kinds of devices are the laterally driven comb-drive polysilicon micro resonators (Tang et al 1989), Analog Device's integrated polysilicon ADXL-50 accelerometers (Analog Device Inc. 1991), flexural polysilicon micro gyros (Juneau & Pisano 1996), and the cascade 300-kHz micromechanical filters (Wang & Nguyen 1997). In these cases, the micro flows are shear driven (Beskok et al 1996) instead of pressure driven, as in the channel and nozzle flows.

Air damping in microstructures is an underexplored but important issue, because it directly influences the quality (Q) factor, of the devices. For example, it has been shown (Nguyen 1995) that the Q factor of a polysilicon resonator can be as high as 100,000 in vacuum but drops to 100 in atmospheric air. This actually illustrates that air damping may be the most important factor when compared to other effects like thermal vibration and fatigue. The strong air damping is due to the dramatic increase in surface-to-volume ratio.

In order to systematically investigate air damping, the air pressure is divided into three regions (Newell 1968). In the first region where the pressure is in low vacuum, air damping is negligible when compared to the intrinsic damping (internal friction) within the resonator. Experimentally, this region happens roughly below 10–100 Pa for microresonators. The damping in this region is largely dependent on the surface-to-volume ratio, the surface quality (the surface may be more lossy than the bulk material), and the material. In the second region, momentum transfer between the resonator and individual air molecules dominates the damping. Here, little or no interaction between air molecules happens, and a simple model has been derived based on the assumption that the rate of momentum transfer is proportional to the difference in velocity between the air molecules and the resonators (Christian 1966). The result is that the Q factor is inversely proportional to the ambient pressure ($Q \cong 1/p$). This region typically ends around 10^3 Pa. In the third region, the pressure is high enough that air molecules do interact with each other, and viscous damping dominates the behavior of the resonators. In this region, the Q factor is inversely proportional

to the fluid viscosity ($Q \cong 1/\mu$). The boundary condition must change from slip to non-slip flow when the surrounding pressure increases. What is the Knudsen number for this change in the boundary condition? Do other surface forces play a role in resonator performance? There is not enough experimental evidence to answer these questions yet.

When the viscous damping of laterally driven microstructures was studied (Zhang & Tang 1994), it was found that the simple Couette and Stokes flow model can significantly underestimate the damping in microstructures, and that this discrepancy is larger for smaller resonators. Most of the microstructures have a complex configuration. For example, the comb structure and the surrounding walls can also play an important role. The detailed geometry of the device (e.g. the resonator's thickness and edges) needs to be considered for more accurate modeling.

An example illustrating the importance of the geometry details is the dynamic response of a thin squeeze-film. In a numerical simulation of a micro accelerometer (Yang & Senturia 1996), the squeeze-film in a low air-pressure environment has a frequency response about four orders of magnitude better than that at atmospheric pressure conditions. When the geometry is slightly altered by placing small etching holes through the accelerometer film, the flat portion of the frequency response is extended by three decades beyond that of a solid film (Figure 9).

The displacement of some MEMS devices can be much larger than their transverse dimension. Other interesting air-damping problems arise. A flap device (Miller et al 1996) driven by an electromagnetic field has an off-plane displacement 1000 times larger than the thickness of the flap. The measured Q factors depend on the magnitude of the displacement. It is believed that the nonlinear viscous damping contributes to this phenomenon. This again is a rather unexplored issue.

4.6 *Micro Flow Diagnosis*

Measuring flow properties in a micro configuration is a challenging task, because the sensors need to be much smaller than the size of the device under study. In addition, the momentum and the energy of the flow is very small. For example, the kinetic energy flux in the channel with helium flow (Figure 2) is about 5.4×10^{-13} J/s for inlet pressure at 20 psig. Therefore, only an extremely small amount of momentum and energy exchange between flow and sensor is allowed so as not to alter the flow. For these reasons, a very limited number of sensors have been developed for micro flow measurements.

The micro channel with integrated pressure sensors (Figure 2) is one example. A very small duct (0.25 micron high and 1 micron wide) is used to connect

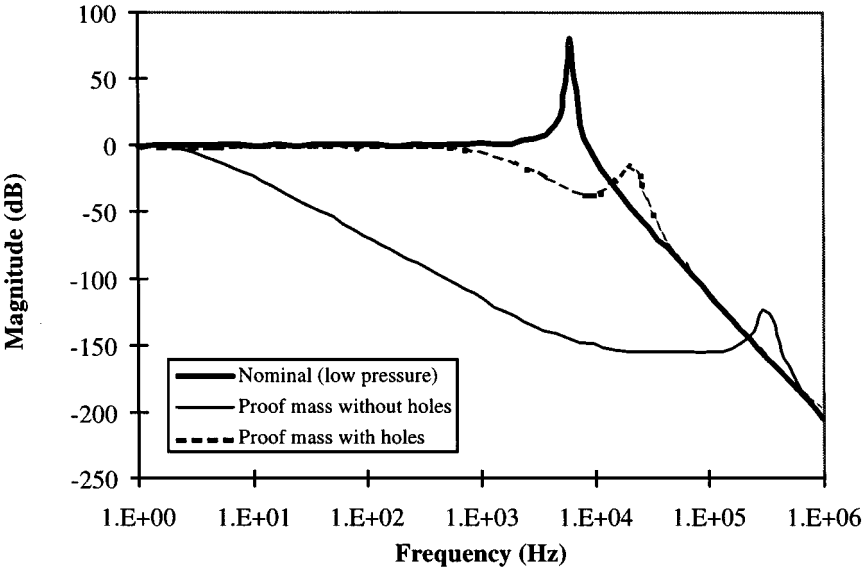

Figure 9 The dynamic response of a thin squeeze-film (Yang & Senturia 1996).

not-very-small micro sensors (compared to the size of the channel) to the channel for increased spatial resolution. Time-averaged pressure can be obtained by this arrangement. If unsteady pressure data are needed, questions about the calibration procedures and even the physical meaning of the data may arise. Furthermore, even though the pressure sensor has a high frequency response, we do not know the constraints of the small duct imposed on the unsteady pressure field. For temperature measurement, thermocouples of 4 microns $\times$ 4 microns have been developed for measuring surface temperature along a 20-micron channel (Figure 10; Zohar et al 1996). In high Knudsen-number flows, a temperature jump can occur between the wall and the bulk flow. Fabricating an in-flow temperature sensor without introducing large disturbances to the micro flow is not a trivial task.

Flow visualization has been proven to be a very useful technique in macro fluid-dynamics research, and extensive effort has been expended on developing methods for visualizing flow in micro channels and valves (Lanzillotto et al 1996). The wavelength of visible light is not short enough for this purpose, so X rays (with wavelengths of 0.62 angstrom) generated by a synchrotron are used. An advantage is that they can be utilized for visualizing flows behind certain silicon structures, such as polysilicon, which are not transparent to visible light.

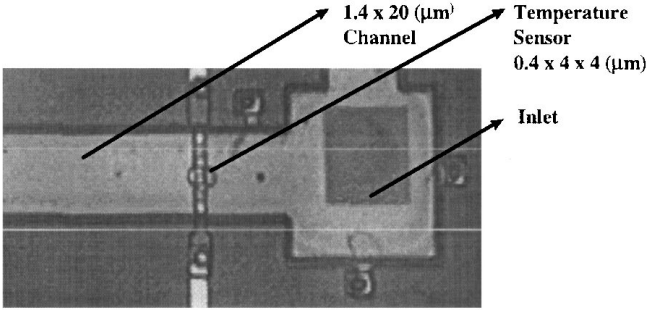

Figure 10 The in-situ temperature sensor in a micro channel (Zohar et al 1996).

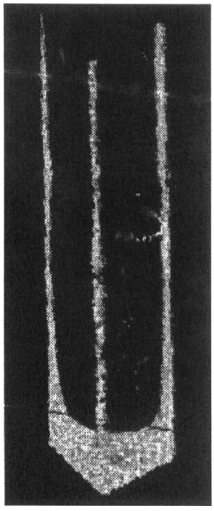

Figure 11 Flow visualization by X ray in a micro channel (Lanzillotto et al 1996).

Figure 11 shows the motion of a water/air interface during a filling process inside a 100-micron-deep by 140-micron-wide channel with a triangular cross section. Water climbs along the sharp corners of the triangle at a rate that is so fast that it is beyond the resolution limit of the current technique. The meniscus surface in the middle of the channel is left far behind the corner interface. This phenomenon is caused by the large surface-tension force associated with the extremely small corner curvature of the micro channel.

5. FLOW TRANSDUCERS

A typical micro transducer is about 100 microns in size, which is at least one order of magnitude smaller than traditional transducers. The improvement in spatial resolution comes naturally, because the significant reduction of inertial mass and thermal capacity can increase the frequency response to an unheard-of range [>1 MHz for a micro hot-wire (Jiang et al 1994)]. The lithographic process and the small size enable us to use 100, 1000, or even more transducers for sensing and/or controlling a phenomenon that has distributed features, such as the high-speed streaks in a turbulent boundary layer.

However, a few problems are associated with using multiple transducers. Traditionally, the leads of each transducer are connected to an external signal-conditioning instrument. Handling 100s or 1000s of signal paths is tedious and usually prohibitive. In addition, these leads occupy a large portion of the precious surface area on the chip. For example, the surface shear-stress sensor array containing 85 sensors (Ho et al 1997; see Figure 18, color insert) only takes about 1% of the area, whereas the leads occupy about 50% of the surface.

Another problem is the limitation in signal bandwidth. Depending on the number of transducers used, we may sometimes not be able to take full advantage of the high-frequency response. However, these problems can be alleviated by integrating the signal conditioning and even decision circuits with the micro transducers in such a way that the leads can be connected locally and thereby significantly reduce the required surface area. The output and input then can be only a few wires. Furthermore, the local circuit wire only processes the output from one or a few transducers, so bandwidth limitation will no longer be a problem. However, the signal processing circuitry still needs to be kept simple. It is not feasible to integrate a powerful microprocessor with each sensor–actuator pair in a large transducer array. Neural networks are a feasible approach, and numerical (Lee et al 1997) experiments show successful examples of using simple neural network–based processing for controlling transitional or turbulent flows.

Another issue is the energy expenditure of the transducers. In the case of flow control, we usually need to have a net energy saving for the whole system. Typically, the energy requirement for a micro flow sensor can be kept around a few milliwatts, but the energy expended for micro actuators is usually much higher. Improvements in this area are clearly needed.

5.1 *Micro Flow Sensors*

5.1.1 HOT-WIRE ANEMOMETERS Micro-machined polysilicon hot wires (Jiang et al 1994) can have a cross-section as small as $0.5 \times 0.5\ \mu\text{m}^2$ and a length of from one to several-hundredths microns (Figure 12). A significant increase in

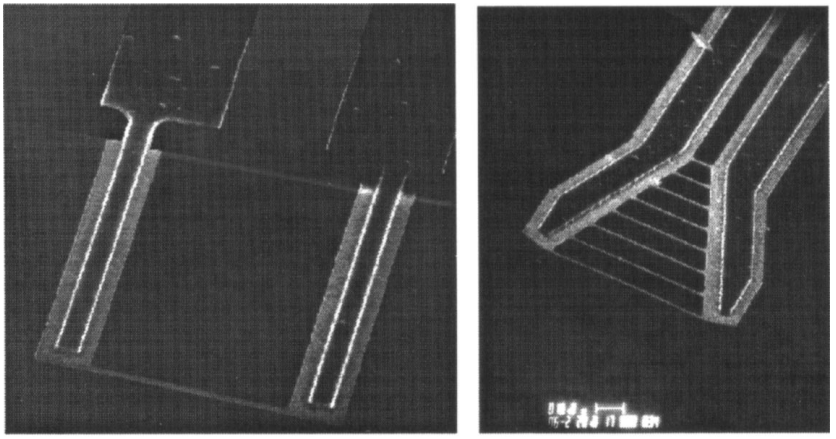

Figure 12 Micro hot wires: (*a*) a 1-μm $\times$ 70-μm single hot wire; (*b*) a hot-wire array (Jiang et al 1994).

spatial resolution can be achieved. Using polysilicon has many other advantages. One is that the temperature coefficient of resistance (TCR) of polysilicon can be varied from -2% to 0.2%/°C using a range of doping concentrations of boron or phosphorus from 10^{17} to 10^{20} atoms/cm^3. In comparison, conventional platinum wires only have a TCR of around 0.1%/°C. We can use such a large variation of the TCR of polysilicon to design a hot wire that specifically requires thermal sensitivity.

The other advantage of the polysilicon wire is that a hot wire's time constant is inversely proportional to the wire's resistivity (Blackwelder 1981). Since conventional hot wires use metals exclusively, resistance is typically low (5–30 ohms). On the other hand, the resistance of polysilicon wires can be adjusted over a wide range (from 1 kΩ to several 100 kΩ). When a constant temperature mode is used, a bandwidth of 1.4 MHz has been achieved with the aid of a heavily doped polysilicon wire. These extremely high frequency responses of a micro hot wire are mainly achieved by adjusting their material properties rather than by simply reducing their size.

5.1.2 SHEAR-STRESS SENSORS A thermal-surface shear-stress sensor is a hot film placed on a surface (Haritonidis 1989). This sensor has reasonable sensitivity while it is used in water. When air is the working medium, however, most of the heat is conducted into the substrate rather than into the air because of the very low heat capacity of air. The use of surface-micromachined

shear-stress sensors (Jiang et al 1996, Huang et al 1996) resolved the problem. A polysilicon wire is placed on a 1.2-μm-thick and 200×200-μm^2 silicon-nitride diaphragm. Underneath the silicon-nitride diaphragm is a 2-μm-deep vacuum cavity (Figure 13*a*). Significant thermal insulation has been achieved by using the vacuum chamber and the silicon-nitride diaphragm with low thermal conductivity. Figure 14 shows that the resistance of the polysilicon wire on a vacuum-insulated diaphragm is almost an order of magnitude higher than that on a solid substrate. The micro-surface shear-stress sensor has a sensitivity of 100 mV/Pa and a bandwidth of 10 kHz and higher.

This type of micro sensor can also be integrated into a large array and can even form a flexible skin to be placed on a curved surface (Jiang et al 1997). Mechanically, the flexible skin (Figure 13*b*) consists of 128 separated silicon "islands" (1 mm $\times$ 1 mm $\times$ 80 μm) that are connected together by a thin polyimide film (1/20 μm thick). The shear-stress sensors are built on the silicon islands. This skin has been taped on a semi-cylindrical (1.3-cm-diameter) delta-wing leading edge to perform real-time 2-D shear-stress mapping. Flow separation along the leading edge has then been successfully measured using the skins.

A different design of a thermal-based wall shear-stress micro sensor has been reported by Löfdahl et al (1996). In this case, the sensor is a $300 \times 60 \times 30$-μm^3 silicon chip that uses a temperature-sensitive silicon diode as the temperature

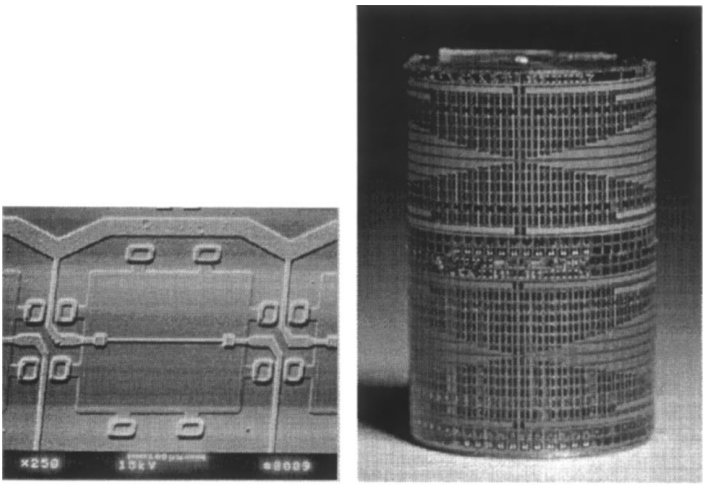

Figure 13 Micro-surface shear-stress sensor (Jiang et al 1996 & 1997). (*a*) a single sensor; (*b*) a flexible array of 128 sensors.

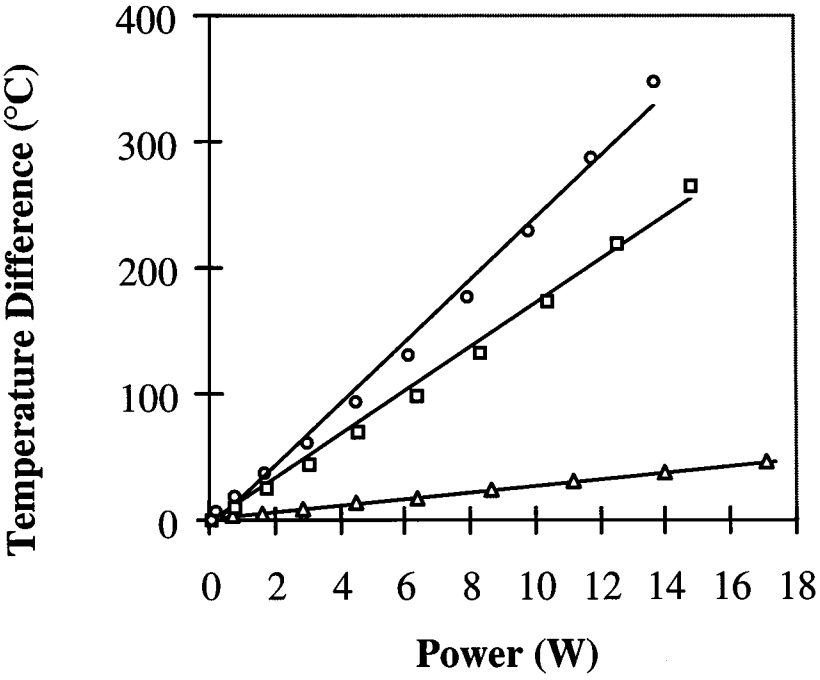

Figure 14 Heating element temperature of the shear-stress sensor (Jiang et al 1994). ○ = heating element on vacuum chamber; □ = heating element on air-filled chamber; Δ = heating element on solid substrate.

sensing element. This chip is embedded in a silicon diaphragm with polyimide-filled trenches to improve thermal isolation. This device takes about 40 mW of power in order to obtain a biased differential temperature of 100°C. The uniqueness of this work is that a polysilicon-diaphragm piezoresistive pressure sensor is also integrated with the shear-stress sensor.

By suspending a micro floating element, a direct measure of the shear stress can be achieved. Schmidt et al (1988) first reported a micro floating-element shear-stress sensor. It was designed to provide a spatial resolution of 100 μm and a bandwidth of 20 kHz. The floating element was a $500 \times 500 \times 30$-μm^3 polyimide plate tethered by polyimide beams. When exposed to shear stress, the plate movement was sensed capacitively with two integrated field-effect transistors (FET) and off-chip electronics. A sensitivity of 52 μV/Pa was reported.

Pan et al (1995) then reported a different floating element. Pan's device is made of thin-film polysilicon. A typical device includes a polysilicon floating

element ($\sim 100 \times 100 \times 2.2\ \mu m^3$) and several suspension beams ($\sim 100\ \mu m$ long). These floating elements have much smaller sizes and better sensitivities (167 mV/Pa), owing to delicate force-balance electronics. Padmanabhan et al (1995) reported a single crystalline-silicon bulk-micromachined and silicon-fusion-bonded sensor. The movement of the element is measured by two photo diodes underneath the element.

5.1.3 PRESSURE SENSORS Micro piezoresistive pressure sensors represent the most mature and successful application of MEMS devices, having a wide range of applications from automobiles to biomedical instruments. Micromachined piezoresistive silicon-based pressure sensors were first introduced in 1958 by Kulite, Honeywell, and MicroSystems (Brysek et al 1990). At that time the devices were typically made with silicon piezoresistors glued to metal diaphragms. The much more advanced micro-pressure sensors used today are made by anisotropic etching of silicon, which requires no hand assembly. Examples are the fully integrated Motorola pressure sensor (Fraden 1993) and the silicon-fusion-bonded millimeter– and submillimeter–size pressure sensors (Brysek et al 1990).

Polysilicon has been a popular material for piezoresistive pressure sensors, but many diaphragm materials have been explored, such as polysilicon (Guckel et al 1986, Sugiyama et al 1991) and silicon nitride (Liu et al 1995). A wide range of piezoresistive pressure sensors is available, up to 10,000 psi, and typical uncompensated full-scale pressure sensitivity is about 20 mV/V. Capacitive pressure sensors have the advantages of better sensitivity and less temperature drift (Lee & Wise 1982, Ko et al 1982). Their performance, however, depends heavily on electronics.

5.1.4 TEMPERATURE SENSORS Many different temperature sensors have long been available (Fraden 1993), and most of these temperature-sensing schemes can be implemented in micro scales. For example, the silicon-resistive and pn-junction temperature sensors are widely used for temperature compensation in silicon diaphragm-type pressure sensors (Brysek et al 1990). An interesting example is an infrared (IR) detector that uses a thin diaphragm to absorb incoming IR light, converting the photon energy into heat (Lahiji & Wise 1980). On the $2 \times 2\text{-mm}^2$ diaphragm ($1\ \mu m$ thick), a large number of thin-film thermal couples (Bi–Sb and Au–polysilicon) that are connected in series to amplify the signal were fabricated. The device shows an impressive sensitivity of 30 V/W and a time constant below 10 ms.

5.2 *Micro Flow Actuators*

Several actuating mechanisms, including electrostatic, electromagnetic, thermopneumatic, etc. are used in micro actuators. Among them, electrostatic

actuation is most popular, mainly because of its ease of fabrication. However, the electrostatic actuation has intrinsic limitations of force ($\sim\mu$N) and displacement ($\sim\mu$m) outputs. They can be used to study flow instability problems where only small displacement is required. For example, Huang et al (1996) made an electrostatic actuator to control screech in high-speed jets. With the design of 70-μm peak-to-peak displacement at the resonant frequency of 5 kHz of the device, it has been shown that proper disturbances in the jet flow can be provided.

Electromagnetic actuation can provide much larger forces (100s of μN) and higher displacements (mm). For example, a micro-magnetic flap (Miller et al 1996) with a 30-turn copper coil and a layer of Permalloy ($Ni_{80}Fe_{20}$) was fabricated on a 4 $\times$ 4-mm^2 silicon plate (40 μm thick). In a magnetic field of 1 kg, the device can be driven to a rotational angle of more than 30°, because of the induction of magnetization in the Permalloy. In addition, a $\pm$100 mA of current can then be applied to the coil to move the flap another $\pm$10°. This allows total control of the flap for more than 2 mm of tip motion (Figure 15). These and other similar devices have been shown to be effective in changing the separation of a flow around a leading edge (Liu et al 1995) and to achieve drag reduction in boundary layer flow (Tsao et al 1994, Ho et al 1997).

The thermopneumatic actuation mechanism is a technique that can provide force (>N) and displacement (>mm) even larger than that of the electromagnetic method. Thermopneumatic actuation, first demonstrated by Zdeblick & Angell (1987), showed that a heater in a liquid-filled cavity can heat the fluid

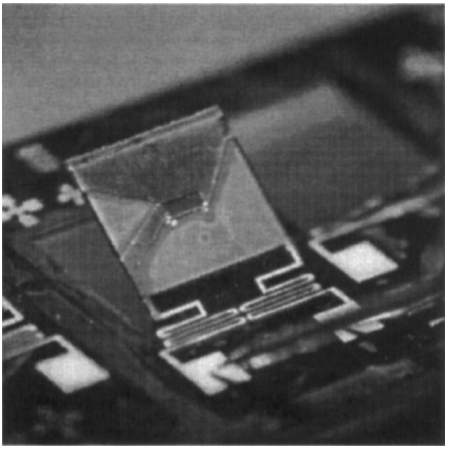

Figure 15 Micro electromagnetic flap actuator (Miller et al 1996).

and cause significant pressure inside the cavity. If a wall of the cavity is a diaphragm, it will be pushed outward because of the differential pressure increase. Because the pressure increase can easily be several psi, the force acting on the diaphragm is large. However, an earlier demonstration used only flat silicon diaphragms, so the deflection was limited by the mechanical structures. A recent demonstration that used a silicone rubber diaphragm showed more than a mm displacement with about 10 psi pressure (Yang et al 1997). It is foreseeable that such an actuator may have important applications in flow actuation.

6. FLOW CONTROL BY MICRO SYSTEMS

A micro system that contains transducers and/or logic circuitry is capable of sensing, signal processing, and actuation. Such a system obviously has numerous engineering applications (Gad-el-Hak 1993, Ho & Tai 1996, McMichael 1996, Ho et al 1997). A few examples of using micro systems for flow control are reviewed here.

6.1 *Moment Control of a Delta Wing*

On a delta wing, the two leading-edge separation vortices contribute up to 40% of the lift at high angles of attack. If we can break the symmetry of these vortices, a net rolling torque may be achieved that can be used for maneuvering the wing. Leading edge vortices develop from a boundary layer separated from the surface. In free shear flows, it has been demonstrated that minute perturbations at its origin can globally modify the flow field (Ho & Huang 1982, Oster & Wygnanski 1982). Therefore, a coupling between micro actuators and wing-size flow structures can be made by manipulating the thin boundary layer.

A delta wing with a 56.5° sweep angle was used in this experiment (Lee et al 1996). Electromagnetically driven microactuators are placed along the leading edges with a circular cross section. The location of the actuators on the leading edge is indicated by an angle, θ, which is measured from the lower surface, $\theta = 0^\circ$, and of the wing toward the upper surface, $\theta = 180^\circ$. The measured rolling torques are normalized by the torque produced by the vortex lift, M_v, which is the product of the lift generated by a single leading-edge vortex and the distance between the centroid of the half wing and the center chord. The magnitude of the maximum torque reaches 15% of M_v at $\sim \theta = 60^\circ$ for small actuators (Figure 16). When the actuators match the thickness of the boundary layer, the maximum normalized torque can be about 40% (Ho et al 1997). A flexible skin containing 128 sensors (Figure 13*b*) is used to measure the surface shear stress. The measurements show that the flow separates immediately downstream from $\theta = 60^\circ$. A negative torque was found for actuators placed around $\theta = 80^\circ$. When actuators are placed on both leading edges but at two

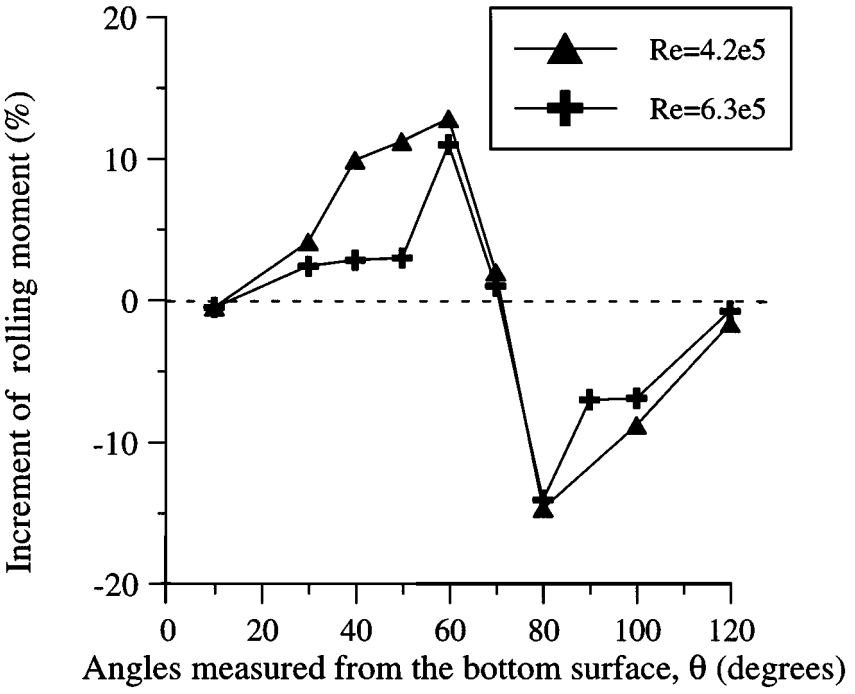

Figure 16 Normalized rolling moment versus actuator location at angle of attack of 25°.

angles ($\theta = 60°, 80°$), the measured resultant torque is equal to the sum of the two peaks. Therefore, the two vortices act independently on this delta wing with a sweep angle of 56.5°. Interactions of the two leading-edge vortices are expected for wings with a larger sweep angle (Lee & Ho 1990). Pitching and yawing torques can also be obtained by using the miniature actuators (Ho et al 1997).

6.2 *Thrust Vectoring*

Deflecting the momentum of a jet to a direction other than the one normal to the nozzle plane is useful in applications such as fluidic switching and aircraft maneuvering. Coe et al (1994) used a micromachined vibrating diaphragm driven by electrostatic force under a cavity to generate a miniature jet. This jet is established by asymmetric entrainment during the push–pull phase. In the pushing phase, the fluid near the jet axis is moved away from the diaphragm. When the diaphragm is pulled back, fluid all around the cavity flows toward the diaphragm and a net concentrated jet flow is established. Acoustical experts

refer to this phenomenon as a "quartz wind" (Kuttruff 1991), because quartz has been used as the diaphragm material in acoustic transducers. When the micro jets are placed at the nozzle of a rectangular jet with a 7.62-cm $\times$ 1.27-cm nozzle, the direction of the large jet can be changed according to the amplitude of the micro jets (Figure 17). This capability provides a simple thrust-vectoring technique (Smith & Glezer 1997), which is obviously much more advantageous than the present method of using paddles to deflect the jet. The paddles suffer high static and dynamic loading, which causes frequent structural damage.

6.3 *Control of Turbulent Skin-Friction*

The discovery of organized structures (Brown & Roshko 1974) has significantly facilitated turbulence control of free shear flows (Ho & Huang 1982, Oster & Wygnanski 1982). However, attempts in the control of wall flows have been much less successful. The dynamics of the large-scale structures in free shear flows are relatively well understood (Ho & Huerre 1984, Huerre & Monkewitz 1990) through the instability process. The underlying mechanisms by which the organized structures are produced and sustained in wall flows are less well known (Robinson 1991). The roots of the problem for experimental studies are (*a*) the transverse length scale of the streaks is on the order of 100s of microns; (*b*) the lifetime of the streaks is about one ms or less; and (*c*) the streaks spread over the entire surface area covered by the turbulent boundary layer.

Their smallness directly poses great difficulties, because traditional transducers are larger than the organized structures. These relatively large transducers do not have enough spatial resolution to measure the structures' properties and to explore their response to perturbations. We cannot devise control schemes

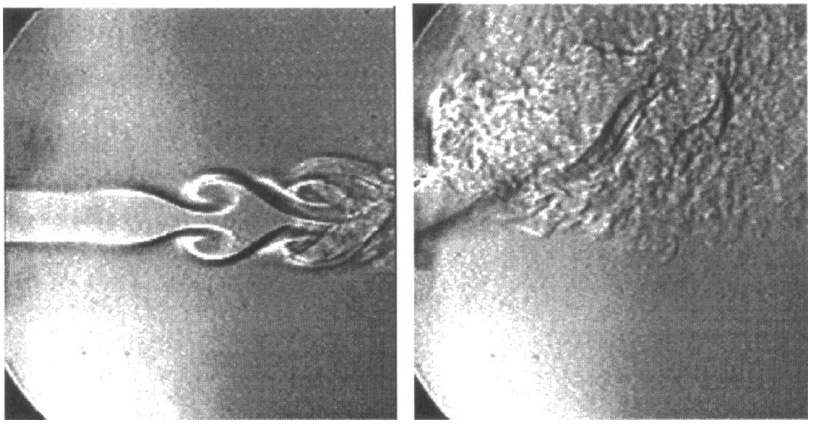

Figure 17 Thrust vectoring by a micro jet (Smith & Glezer 1997).

analogous to research we have done in the past on free-shear layers. The micromachined transducers match the size of the streaks, and integrated logic circuitry enables real-time decisions. A micro system provides an opportunity that makes it possible for the first time to directly manipulate individual wall structures. That is the reason wall-bounded turbulent-flow control is chosen as a testbed for developing a micro system that comprises sensors, logic circuitry, and actuators.

6.3.1 DISTRIBUTED MEASUREMENTS A surface shear-stress imaging chip comprising 85 micro sensors was developed to measure the instantaneous turbulent shear stress in a distributed manner. The size of the sensors and the spacing between them are chosen to match the length scale of near-wall, stream-wise streaks in the tested Reynolds-number range. Figure 18 (see color insert) shows the instantaneous surface shear-stress contours measured by the sensor array. Only 25 sensors in a linear spanwise array are used. The vertical direction is a pseudo-streamwise plot generated by multiplying time by the convection speed. The capability of measuring the surface shear stress is not only essential for the interactive control of the high-speed streaks but also provides interesting statistical properties of the streaks (Motoaki et al 1997).

6.3.2 INTERACTION BETWEEN THE ACTUATOR AND WALL STRUCTURES Being able to perform distributed sensing is a major step forward. Understanding how the actuator interacts with the near-wall structure is an even more important part of the control process. Actuators are wall-mounted devices that can produce surface deformation and/or flow disturbances. The flow altered by a rising obstacle was studied by direct numerical simulation (Carlson & Lumley 1996). Vortical structures are produced by the unsteady motion of the actuator and are deformed while the actuator moves through the boundary-layer velocity shear. These actuator-produced perturbations are expected to alter the near-wall structure in such a way that a skin-friction reduction is achieved. Obviously, realizing this concept depends on finding proper actuation commands, which in turn requires an in-depth understanding of the nonlinear interaction between the artificial disturbance and the high-speed streaks. However, almost all of the experiments at present investigate the effect of an actuator on stationary vortices embedded in a laminar flow (Jacobson & Reynolds 1995, Ho & Tai 1996), because studies of the effect on the streaks in turbulent flow require a complete micro system (see Section 6.3.3), which is still under development.

At the entrance region of a 2-D channel flow, the boundary layer is laminar. A 1.3-mm-thick bump was placed normal to the flow and terminated halfway in the span-wise direction (Ho & Tai 1996). At the terminating position of the bump, a stationary longitudinal-vortex pair was produced. A micromachined

actuator (Figure 16), which is a silicon nitride flap driven by an electromagnetic field, was placed downstream of the vortex generator. During the upward-moving phase, the ensemble-averaged vertical velocity field (Figure 19) shows the transport of high-velocity fluid away from the surface. It is interesting to note that the downward motion of the actuator does not produce a symmetric cancellation effect. Because of the presence of the wall, the low-speed fluid under the flap is pushed upward during the downward motion of the flap so that a net reduction in the skin drag is achieved through a complete cycle of the flap motion. The surface shear stress was integrated along the spanwise direction and over the whole cycle of the motion of the actuator. The integrated shear stress normalized to the dynamic head is defined as the skin drag coefficient (C_{dv}). If a proper driving signal is applied to the actuator, the skin drag coefficient of the vortex actuator interaction (C_d) is lower than the drag coefficient of the stationary vortex alone. The net reduction of the surface shear stress is the difference between these two coefficients.

The net reductions are plotted for various actuator frequencies (ω) and maximum tip heights (d) in Figure 20. The product of ω and d is the maximum normal velocity of the actuator. For constant ωd, the net reductions in the skin-friction drag are the same for different combinations of ω and d. This result indicates that the amount of shear-stress reduction is directly related to the

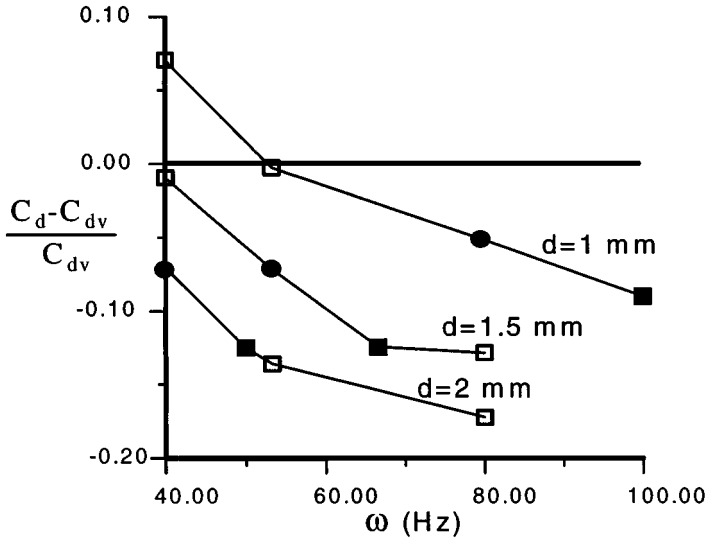

Figure 20 Surface shear-stress reduction as a function of actuator frequency, ω, and maximum actuator tip height, d (Ho et al 1997). ●, ωd = 80 mm/sec; ■, ωd = 100 mm/sec.

ability to transport high-speed fluid. In other words, we need to seek actuators that can efficiently pump high-speed fluid away from the wall with low power expenditure and low form drag.

In a water channel, the interaction between a piezoelectrically driven actuator with a vortex pair developed from a cylinder was studied (Jacobson & Reynolds 1995). Surface-mounted hot-film sensors were used to measure the surface shear stress, which serves as an input for feedback control. The optimum amplitude of the actuator obtained from the feedback control can delay the laminar-turbulent transition to about 40 displacement thicknesses from the natural transition region (Figure 21).

6.3.3 A MICRO SYSTEM FOR SURFACE SHEAR-STRESS REDUCTION The lifetime of high-speed streaks is short, and many of the streaks need to be controlled simultaneously. If all of the sensor outputs were to be sent to a central computer and the control command were to be sent from the computer to each actuator, a very high bandwidth signal path and large number of leads would be required.

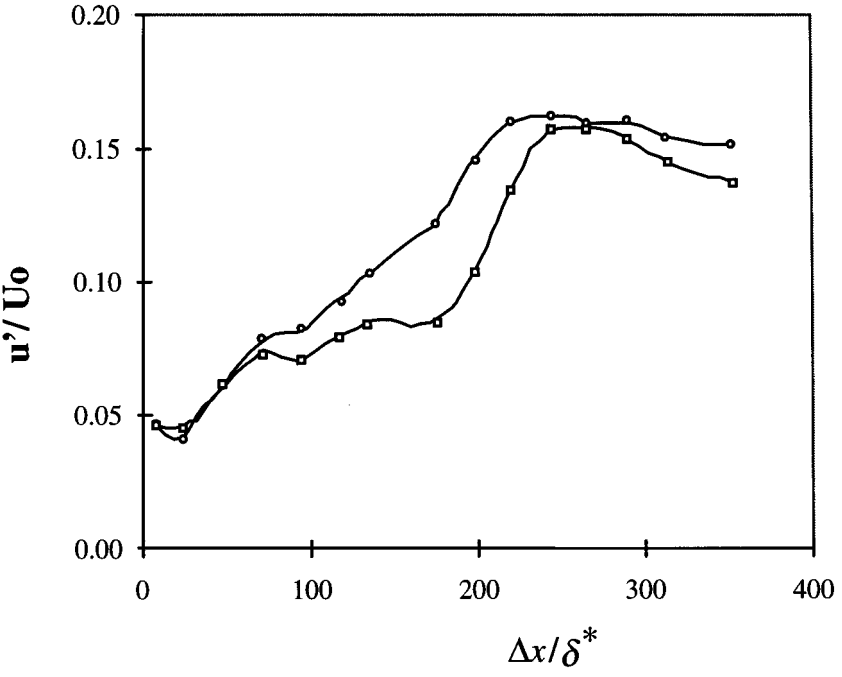

Figure 21 Transition delay by actuation (Jacobson & Reynolds 1995). δ = displacement thickness.

Implementing local and simple signal processing is obviously a necessity for alleviating these problems. Neural networks are a viable approach (Jacobson & Reynolds 1995, Lee et al 1997). A neural network–based circuit was developed to determine the time and the spatial extent of the high-speed streaks passing the shear-stress-sensor array (Gupta et al 1996). The output of the circuit was used for actuation.

The task of integrating a micro system containing micro sensors, microelectronics, and micro actuators on a chip is possible, yet it is not trivial. The micro transducers that integrate the circuit need to be fabricated at a much higher temperature than that of the circuits, which means that the diffusion of the doping material in the circuits may affect their performance. The process flow needs to be carefully planned to eliminate cross-contamination. A micro system for shear-stress reduction was fabricated on a 1-cm $\times$ 1-cm die; 18 micro shear-stress sensors, 3 micro flap actuators, as well as circuits for logic sensor drivers and actuator drivers are monolithically integrated (Figure 22). This is a prototype, and various tests of its functionalities are under way.

7. CONCLUDING REMARKS

The ability to apply a large number of transducers with on-board signal processing provides a paradigm shift for flow control. This type of micro system enables us to perform real-time distributed control. Hence, the ability to interactively manipulate individual high-speed streaks in the turbulent boundary layer is made possible and could be effective in decreasing the surface friction force. A near-term industrial application for the skin-friction-drag experiment is not obvious. This approach, however, will definitely facilitate our exploration of the near-wall structure under artificial perturbations, and the findings will lead us toward a fundamental understanding of the grand challenge in turbulence research. Furthermore, other types of flow control may also be inspired by the real-time, distributed-control ability of MEMS-based transducers. The large torque on a delta wing and the thrust vectoring achieved by microactuation are examples. We expect that a stream of new flow phenomena will be introduced by MEMS-based sensing and control schemes.

In the field of biomedical analysis, MEMS technology has already sparked a major transformation. Flows through micro channels or nozzles are the most common configurations in all of the biomedical applications. Many unexpected phenomena have been observed in Newtonian fluid flows through these simple configurations. These types of flows are extremely intriguing, because they challenge the fundamentals of fluid dynamics: the non-slip boundary condition clearly should be relaxed for gas flows. In liquid flows, extra surface-force terms may need to be added to the momentum balance equation. Whether any

modification needs to be made to the constitutive equation for a simple fluid remains to be investigated. On the other hand, the molecular dynamics approach provides another means by which to explore the micro-fluidic problems. It is evident that micro flow has opened a new domain for basic fluid mechanics research.

ACKNOWLEDGMENTS

MEMS is a multidisciplinary field and, as such, cooperation among scientists with different backgrounds is essential to accomplish this work. It is our privilege and pleasure to work with researchers who make these nearly impossible tasks become reality. We thank Professors R Goodman, CJ Kim, J Kim, J Speyer, K Wang, J Woo; Drs. B Gupta, S Joshi, S Tung, Mr. D Babcock, F Jiang, C Lee, GB Lee, C Liu, J Shih, and T Tsao. This work is supported by Dr. J McMichael of AFOSR, as well as Drs. K Gabriel and M Francis of DARPA. Their willingness to take risks is a key factor enabling the research community to unveil the exciting Aero-MEMS area.

Literature Cited

Analog Device Inc. 1991. *ADXL50 Catalog*
Arkilic E, Breuer KS. 1993. Gaseous flow in small channels. *AIAA Pap. 93–3270*
Arkilic E, Schmidt MA, Breuer KS. 1995. Gaseous slip flow in long microchannels. *J. MEMS* 6:167–78
Beskok A, Karniadakis GE. 1992. Simulation of slip-flows in complex micro-geometries. *ASME DSC* 40:355–70
Beskok A, Karniadakis GE. 1993. Simulation of heat and momentum transfer in complex micro-geometries. *AIAA Pap 93–3269*
Beskok A, Karniadakis GE, Trimmer W. 1996. Rarefaction and compressibility effects in gas microflows. *J. Fluids Eng.* 118:448–56
Blackwelder RF. 1981. Hot-wire and hot-film anemometers. In *Methods of Experimental Physics: Fluid Dynamics*, ed. RJ Emrich, 18:259–314. New York: Academic
Brown GL, Roshko A. 1974. On density effects and large structure in turbulent mixing layers. *J. Fluid. Mech.* 64:775–816
Brysek J, Petersen K, Mallon J, Christel L, Pourahmadi F. 1990. *Silicon Sensors and Microstructures*. San Jose, CA: NovaSensor
Carlson HA, Lumley JL. 1996. Flow over an obstacle emerging from the wall of a channel. *AIAA J.* 34:924–31
Christian RG. 1966. The theory of oscillating-vane vacuum gauges. *Vacuum* 16:175–78
Coe DJ, Allen MG, Trautman MA, Glezer A. 1994. Micromachined jets for manipulation of macro flows. In *Tech. Dig. Proc. Solid-State Sens. Actuator Workshop, Hilton Head Isl., SC*, pp. 243–47. Cleveland Heights, OH: Transd. Res. Found.
Dussan EB, Davis SH. 1974. On the motion of fluid-fluid interface along a solid surface. *J. Fluid Mech.* 65:71–95
Eddington AS. 1928. *Nature of the Physical World*. Cambridge/London/New York: Cambridge Univ. Press
Fan LS, Tai YC, Muller RS. 1988a. IC-processed electrostatic micromotors. In *Tech. Dig. Int. Electron Dev. Meet. (IEDM), San Francisco*, pp 666–69
Fan LS, Tai YC, Muller RS. 1988b. Integrated movable micromechanical structures for sensors and actuators. *IEEE Trans. Electron Devices* 35:724–30
Fraden J. 1993. *AIP Handbook of Modern Sensors*. New York: AIP. 552 pp.
Gad-el-Hak M. 1993. Innovative control of turbulent flows. *AIAA Pap. 93–3268*
Guckel H, Burns DW, Rutigliano CR. 1986. Design and construction techniques for planar

polysilicon pressure transducers with piezoresistive read-out. In *Tech. Dig. Proc. Solid-State Sens. Actuator Workshop, Hilton Head Isl., SC,* pp. 79–79. Cleveland Heights, OH: Transd. Res. Found.

Gupta B, Goodman R, Jiang F, Tai YC, Tung S, Ho CM. 1996. Analog VLSI system for active drag reduction. *IEEE Micro.* 16:53–59

Haritonidis JH. 1989. The measurement of wall shear stress. In *Advances in Fluid Mechanics Measurements,* ed. M Gad-el-Hak, pp. 229–61. Berlin/Heidelberg/New York: Springer-Verlag

Harley JC, Huang Y, Bau H, Zemel JN. 1995. Gas flow in micro-channels. *J. Fluid Mech.* 284:257–74

Hasegawa T, Suganuma M, Watanabe H. 1997. Anomaly of excess pressure drops of the flow through very small orifices. *Phys. Fluids* 9:1–3

Ho CM, Huang LS. 1982. Subharmonics and vortex merging in mixing layers. *J. Fluid Mech.* 119:443–73

Ho CM, Huerre P. 1984. Perturbed free shear layers. *Annu. Rev. Fluid Mech.* 16:365–424

Ho CM, Tai YC. 1996. MEMS and its applications for flow control. *J. Fluids Eng.* 118:437–47

Ho CM, Tung S, Lee GB, Tai YC, Jiang F, Tsao T. 1997. MEMS—A technology for advancements in aerospace engineering. *AIAA Pap. 97–0545*

Howe RT, Muller RS. 1983. Polycrystalline silicon micromechanical beams. *J. Electrochem. Soc.* 130:1420–23

Huang C, Papp J, Najafi K, Nagib H. 1996. A microactuator system for the study and control of screech in high speed jets. In *An Investigation of Micro Structures, Sensors, Actuators, Machines, and Systems.* Proc. Ann. Int. Workshop MEMS, 9th, Amsterdam, pp.19–24. New York: IEEE

Hunter RJ. 1981. *Zeta Potential in Colloid Science: Principles and Applications*. New York: Academic. 386 pp.

Huerre P, Monkewitz PA. 1990. Local and global instabilities in spatially developing flows. *Annu. Rev. Fluid Mech.* 22:473–537

Israelachvili J. 1991. *Intermolecular and Surface Forces*. New York: Academic. 450 pp. 2nd ed.

Jacobson SA, Reynolds WC. 1995. An experimental investigation towards the active control of turbulent boundary layers. *Stanford Univ. Rep. TF–64,* Palo Alto, Calif.

Jiang FK, Tai YC, Gupta B, Goodman R, Tung S, Huang J, Ho CM. 1996. A surface-micromachined shear-stress imager. In *An Investigation of Micro Structures, Sensors, Actuators, Machines, and Systems*. Proc. Ann. Int. Workshop MEMS, 9th, Amsterdam, pp. 110–15. New York: IEEE

Jiang FK, Tai YC, Ho CM, Li WJ. 1994. A micromachined polysilicon hot-wire anemometer. In *Tech. Dig. Proc. Solid-State Sens. Actuator Workshop, Hilton Head Isl., SC,* pp. 264–67. Cleveland Heights, OH: Transd. Res. Found.

Jiang FK, Tai YC, Walsh K, Tsao T, Lee GB, Ho CM. 1997. A flexible MEMS technology and its first application to shear stress sensor skin. In *An Investigation of Micro Structures, Sensors, Actuators, Machines, and Robots*. Proc. Ann. Int. Workshop MEMS, 10th, Nagoya, pp. 465–70. New York: IEEE

Joo Y, Dieu K, Kim CJ. 1995. Fabrication of monolithic microchannels for IC chip cooling. In *An Investigation of Micro Structures, Sensors, Actuators, Machines, and Systems*. Proc. Ann. Int. Workshop MEMS, 8th, Amsterdam, pp. 362–67. New York: IEEE

Judge JS. 1971. A study of the dissolution of SiO_2 in acidic fluoride solutions. *Solid-State Sci.* 118:1772–5

Juneau T, Pisano AP. 1996. Micromachined dual input axis angular rate sensor. *Tech. Dig. Proc. Solid-State Sensor Actuator Workshop* pp. 299–302

Kennard EH. 1938. *Kinetic Theory of Gases*. New York: McGraw-Hill. 483 pp.

Knudsen M. 1909. Die Gesetze der molecular Stromung und die inneren Reibungstromung der Gase durch Rohren. *Ann. Phys. (Leipzig)* 28:75–130

Ko WH, Bao MH, Hong YD. 1982. High-sensitivity integrated-circuit capacitive pressure sensors. *IEEE Trans. Electron Dev.* 29(1):48–56

Koplik J, Banavar JR, Willemsen JF. 1989. Molecular dynamics of fluid flow at solid surfaces. *Phys. Fluids A* 1:781–94

Koplik J, Banavar JR. 1995. Continuum deductions from molecular hydrodynamics. *Annu. Rev. Fluid Mech.* 27:257–92

Kuttruff H. 1991. *Ultrasonics Fundamentals and Applications*. London/New York: Elsevier. 452 pp.

Lahiji GR, Wise KD. 1980. A monolithic thermopile detector fabricated using integrated-circuit technology. In *Proc. Int. Electron Dev. Meet., Washington, DC,* pp. 676–79. New York: IEEE

Lanzillotto A, Leu TS, Amabile M, Wildes R. 1996. An investigation of microstructure and microdynamics of fluid flow in MEMS. *ASME AD* 52:789–96

Lee C, Kim J, Babcock D, Goodman R. 1997. Application of neural networks to turbulence control for drag reduction. *Phys. Fluids.* In press

Lee GB, Ho CM, Jiang F, Liu C, Tsao T, et al.

1996. Control of roll moment by MEMS. *ASME DA*. Los Angeles: UCLA

Lee M, Ho CM. 1990. Lift force of delta wings. *Appl. Mech. Rev.* 43:209–21

Lee YS, Wise KD. 1982. Batch-fabricated silicon capacitive pressure transducers. *IEEE Trans. Electron Dev.* 29(1):42–47

Liu C, Tsao T, Tai YC, Leu TS, Ho CM et al. 1995. Out-of-plane permalloy magnetic actuators for delta-wing control. In *An Investigation of Micro Structures, Sensors, Actuators, Machines, and Systems*. Proc. Ann. Int. Workshop MEMS, 8th, Amsterdam, pp. 7–12. New York: IEEE

Liu J, Tai YC, Lee J, Pong KC, Zohar Y, Ho CM. 1993a. In situ monitoring and universal modeling of sacrificial PSG etching using hydrofluoric acid. In *An Investigation of Micro Structures, Sensors, Actuators, Machines, and Systems*. Proc. Ann. Int. Workshop MEMS, 6th, Ft. Lauderdale, FL, pp. 71–76. New York: IEEE

Liu J, Tai YC, Pong K, Ho CM. 1993b. Micromachined channel/pressure sensor systems for micro flow studies. In *Transducers '93*. Dig. Tech. Pap. Int. Conf. Solid-State Sensors Actuators, 7th, Yokohama, pp. 995–99. Yokohama: IEEE Jpn.

Liu J, Tai YC, Pong K, Ho CM. 1995. MEMS for pressure distribution studies of gaseous flows in microchannels. In *An Investigation of Micro Structures, Sensors, Actuators, Machines, and Systems*. Proc. Ann. Int. Workshop MEMS, 8th, Amsterdam, pp. 209–15. New York: IEEE

Löfdahl L, Kalvesten E, Hadzianagnostakis T, Stemme G. 1996. An integrated silicon based wall pressure-shear stress sensor for measurements in turbulent flows. *ASME DSC MEMS* 59:245–51

Mastrangelo C, Hsu CH. 1992. A simple experimental technique for the measurement of the work of adhesion of microstructures. In *Tech. Dig. IEEE Solid-State Sens. Actuator Workshop, Hilton Head Isl., SC*, pp. 208–12. New York: IEEE

McMichael JM. 1996. Progress and prospects for active flow control using microfabricated electro-mechanical systems (MEMS). *AIAA Pap. 96–0306*

Migun NP, Prokhorenko PP. 1987. Measurement of the viscosity of polar liquids in microcapillaries. *Colloid J. USSR* 49:894–97

Miller R, Burr G, Tai YC, Psaltis D. 1996. Electromagnetic MEMS scanning mirrors for holographic data storage. In *Tech. Dig. Proc. Solid-State Sens. Actuator Workshop, Hilton Head Isl., SC*, pp. 183–86. Cleveland Heights, OH: Transd. Res. Found.

Mohiuddin Mala G, Li D, Dale JD. 1996. Heat transfer and fluid flow in microchannels. *ASME DSC* 59:127–36

Monk DJ, Soane DS, Howe RT. 1993. A review of the chemical reaction mechanism and kinetics of hydrofluoric acid etching of silicon dioxide for surface micromachining applications. *Thin Solid Films* 232:1–12

Motoaki K, Tung S, Hoffelner J, Ho CM, Jiang F, Tai YC. 1997. Turbulent surface shear stress measurement by micro sensor arrays. *Proc. Int. Conf. Sci. Arts*, ed. F Fiedler

Nathanson HC, Newell WE, Wickstrom RA, Davis JR. 1967. Resonant gate transistors. *IEEE Trans. Electron Dev.* 14:117–33

Newell WE. 1968. *Science* 161:1320

Nguyen T-C. 1995. Micromechanical resonators for oscillation and filters. *Proc. IEEE Int. Ultrasonic Symp., Seattle*, pp. 489–99

Oh CK, Oran ES, Cybyk ZC. 1995. Microchannel flow computed with the DSMC-MLG. *AIAA Pap. 95–2090*

Oran ES, Oh CK, Cybyk ZC. 1998. Direct-simulation Monte Carlo—recent advances and applications. *Annu. Rev. Fluid Mech.* 30:403–41

Oster D, Wygnanski I. 1982. The forced mixing layer between parallel streams. *J. Fluid Mech.* 123:91–130

Padmanabhan A, Goldberg HD, Breuer KS, Schmidt MA. 1995. A silicon micromachined floating element shear-stress sensor with optical position sensing by photodiodes. In *Transducers '95: Eurosensors IX*. Dig. Tech. Pap. Int. Conf. Solid-State Sensors Actuators, 8th, Stockholm, pp. 436–39. Stockholm: R. Swed. Acad. Eng. Sci.

Pan T, Hyman D, Mehregany M, Reshotko E, Willis B. 1995. Calibration of microfabricated shear stress sensors. In *Transducers '95: Eurosensors IX*. Dig. Tech. Pap. Int. Conf. Solid-State Sensors Actuators, 8th, Stockholm, pp. 443–46. Stockholm: R. Swed. Acad. Eng. Sci.

Petersen K. 1982. Silicon as a mechanical material. *Proc. IEEE* 70:420–56

Pfahler J, Harley JC, Bau H. 1990. Liquid transport in micron and submicron channels. *Sens. Actuators* A21-A23:431–34

Pfahler J, Harley JC, Bau H, Zemel JN. 1991. Gas and liquid flow in small channels. *ASME DSC* 32:49–60

Piekos ES, Breuer KS. 1995. DSMC modeling of micromechanical devices. *AIAA Pap. 95–2089*

Piekos ES, Breuer KS. 1996. Numerical modeling of micromechanical devices using the direct simulation Monte Carlo method. *J. Fluids Eng.* 118:464–69

Pong KC, Ho CM, Liu J, Tai YC. 1994. Nonlinear pressure distribution in uniform microchannels. *ASME FED* 197:51–56

Preston K. 1972. *Coherent Optical Computers*. New York: McGraw-Hill. 315 pp.
Ristic L, ed. *Sensor Technology and Devices*. 1994. Boston: Artech House. 524 pp.
Robinson SK. 1991. Coherent motions in the turbulent boundary layer. *Annu. Rev. Fluid Mech.* 23:601–39
Schmidt M, Howe RT, Senturia S, Haritonidis JH. 1988. Design and fabrication of a micro-fabricated floating element shear-stress sensor. *IEEE Trans. Electron Devices* 35:750–7
Seidel H. 1987. The mechanism of anisotropic silicon etching and its relevance for micromachining. In *Transducers '87*. Dig. Tech. Pap. Int. Conf. Solid-State Sensors Actuators, 4th, Tokyo, pp. 120–25
Shih JC, Ho CM, Liu J, Tai YC. 1995. Nonlinear pressure distribution in uniform microchannels. *ASME AMD-MD 238*
Shih JC, Ho CM, Liu J, Tai YC. 1996. Monatomic and polyatomic gas flow through uniform microchannels. *ASME DSC* 59:197–203
Smith BL, Glezer A. 1997. Vectoring and small-scale motions effected in free shear flows using synthetic jet actuators. *AIAA Pap. 97–0213*
Sugiyama S, Shimaoka K, Tobata O. 1991. Surface micromachined micro-diaphragm pressure sensors. In *Transducers '91*. Dig. Tech. Pap. Int. Conf. Solid-State Sensors Actuators, 6th, San Francisco, pp. 188–91. Piscataway, NJ: IEEE
Tang WC, Nguyen T-C, Howe RT. 1989. Laterally driven polysilicon resonant microstructures. *Sens. Actuators* 20:25–32
Tsao T, Liu C, Tai YC, Ho CM. 1994. Micromachined magnetic actuator for active fluid control. *ASME FED* 197:31–38
Tuckermann DB, Pease RFW. 1982. Optimized convective cooling using micromachined structures. *J. Electrochem. Soc.* 129(3):98C
Wang K, Nguyen T-C. 1997. High-order micromechanical electronic filters. In *An Investigation of Micro Structures, Sensors, Actuators, Machines, and Robots. Proc. Ann. Int. Workshop MEMS, 10th, Nagoya, Jpn.* pp. 25–30. New York: IEEE
Went FW. 1968. The size of man. *Am. Sci.* 56:400–13
Wolf S. 1990. *Silicon Processing for the VLSI Era*, Vol. 2. Sunset Beach, CA: Lattice. 753 pp.
Yang YJ, Senturia SD. 1996. Numerical simulation of compressible squeezed-film damping. In *Tech. Dig. Proc. Solid-State Sens. Actuator Workshop, Hilton Head Isl., SC*, pp. 76-79. Cleveland Heights, OH: Transd. Res. Found.
Yang X, Grosjean C, Tai YC, Ho CM. 1997. A MEMS thermopneumatic silicone membrane valve. In *An Investigation of Micro Structures, Sensors, Actuators, Machines, and Robots*. Proc. Ann. Int. Workshop MEMS, 10th, Nagoya, pp. 114–18. New York: IEEE
Zdeblick MJ, Angell JB. 1987. A miniature electric-to-fluidic valve. *Tech. Dig., Transducers '87.* pp. 827–29
Zhang X, Tang W. 1994. Viscous air damping in laterally driven microstructures. In *An Investigation of Micro Structures, Sensors, Actuators, Machines, and Systems*. Proc. Ann. Int. Workshop MEMS, 7th, Oiso, Jpn. pp. 199–204. New York: IEEE
Zohar Y, Jiang L, Wong M, Wang Y. 1996. Microchannels with integrated temperature sensors. *Bull. Am. Phys. Soc*. 41:1790

Annual Review of Fluid Mechanics
Volume 30, 1998

CONTENTS